

# Nanoscale

Accepted Manuscript



This is an *Accepted Manuscript*, which has been through the Royal Society of Chemistry peer review process and has been accepted for publication.

*Accepted Manuscripts* are published online shortly after acceptance, before technical editing, formatting and proof reading. Using this free service, authors can make their results available to the community, in citable form, before we publish the edited article. We will replace this *Accepted Manuscript* with the edited and formatted *Advance Article* as soon as it is available.

You can find more information about *Accepted Manuscripts* in the [Information for Authors](#).

Please note that technical editing may introduce minor changes to the text and/or graphics, which may alter content. The journal's standard [Terms & Conditions](#) and the [Ethical guidelines](#) still apply. In no event shall the Royal Society of Chemistry be held responsible for any errors or omissions in this *Accepted Manuscript* or any consequences arising from the use of any information it contains.

## ARTICLE

## The nature of the Fe-graphene interface at the nanometer level

Cite this: DOI: 10.1039/x0xx00000x

M. Cattelan<sup>a</sup>, G. W. Peng<sup>b</sup>, E. Cavaliere<sup>c</sup>, L. Artiglia<sup>a</sup>, A. Barinov<sup>d</sup>, L. T. Roling<sup>b</sup>, M. Favaro<sup>a</sup>, I. Píš<sup>d,e</sup>, S. Nappini<sup>e</sup>, E. Magnano<sup>e</sup>, F. Bondino<sup>e</sup>, L. Gavioli<sup>c</sup>, S. Agnoli<sup>a\*</sup>, M. Mavrikakis<sup>b</sup> and G. Granozzi<sup>a</sup>

Received 00th January 2014,  
Accepted 00th January 2014

DOI: 10.1039/x0xx00000x

www.rsc.org/

The emerging fields of graphene-based magnetic and spintronic devices require a deep understanding of the interface between graphene and ferromagnetic metals. This paper reports a detailed investigation at the nanometer level of the Fe-graphene interface carried out by angle-resolved photoemission, high-resolution photoemission from core levels, near edge x-ray absorption fine structure, scanning tunnelling microscopy and spin polarized density functional theory calculations. Quasi-free-standing graphene was grown on Pt(111), and the iron film was either deposited on top of or intercalated beneath graphene. Calculations and experimental results show that iron strongly modifies the graphene band structure and lifts its  $\pi$  band spin degeneracy.

### Introduction

The study of the interface between graphene (G) and metals is gaining more and more interest due to the emergent applications of G in flexible electronics<sup>1</sup> (e.g. touch screen, foldable OLED) and its potential future use in high frequency transistors and thin film logic devices.<sup>2</sup> All these technologies have in common a massive exploitation of G/metal junctions<sup>3</sup> at different levels of complexity. Therefore, the detailed investigation of these heterointerfaces at the nanoscale is of paramount importance for technological advancement and it is expected to inspire the development of novel devices.

G is also emerging as an ideal platform for future spintronics since it combines long spin lifetime with excellent electron velocity. However, in order to assist the implementation of G/metal systems in spintronic devices, a deep understanding of their electronic, structural and interfacial properties has to be reached. For example, a critical issue still to be addressed for the realization of practical spintronic devices is the effective injection of the spin-polarized electrons in conductive channels.<sup>4,5</sup>

Within this context, a quite versatile approach to tailor interfaces relies on modifying the local properties of the G/substrate interface by intercalation with another species (metal, oxide, gases, etc.).<sup>6,7,8,9</sup> For example, the intercalation of alkali metals,<sup>10</sup> noble<sup>6</sup> and transition<sup>11</sup> metals, semimetals,<sup>12</sup> or gases such as oxygen<sup>13,14,15,16</sup> and carbon monoxide<sup>17,18</sup> beneath G epitaxially grown on transition metal single crystals was used to tune the hybridization between the electronic states of G and

the underlying substrate, either to restore the electronic structure of freestanding G or to induce doping.

Only few studies in literature have focused so far on spectroscopic measurements of the structural, electronic and magnetic properties of G in contact with ferromagnetic metals. One of the best studied cases is the growth of G on Ni(111); in this case, a magnetic moment of 0.05-0.1  $\mu_B$  per atom is induced on carbon, as determined by x-ray magnetic circular dichroism.<sup>19,20,21</sup> On this same system after the intercalation of 1 ML of Fe beneath G, the magnetic moment of carbon was enhanced up to 0.25  $\mu_B$ ,<sup>22</sup> but it was difficult to distinguish exactly the magnetic contribution due to the Ni substrate from the component coming from the Fe intercalated film. Recently, bilayer G films grown on SiC and intercalated with Fe were studied by angle-resolved photoemission spectroscopy (ARPES);<sup>23</sup> however, the experimental ARPES data after iron intercalation were not conclusive to assess the effect of the intercalation layer on the electronic structure. Theoretical studies indicate that the modifications due to the intercalation of a magnetic layer are minimal for multilayer G, whereas in the case of single layer G the band structure is expected to change dramatically.<sup>24</sup> Interestingly, a magnetic Moiré pattern was observed using spin-polarized scanning tunneling microscopy (STM) in cobalt intercalated G grown on Ir(111),<sup>25</sup> demonstrating the presence of rich and complex magnetic phenomena at the G/metal interface. Therefore, a clear disentanglement of the several factors influencing the electronic structure and magnetic properties of G-intercalated metal systems has not been achieved yet.

In this framework, the choice of the substrates for the growth of long range ordered single layer G is critical, as many, like Ni, are ferromagnetic on their own, while others, such as Rh<sup>26</sup> or Pd,<sup>27</sup> are characterized by strong metal-G binding interaction. A weak G-substrate interaction is otherwise more desirable to highlight the effects of a further deposited and intercalated ferromagnetic metal layer on the electronic structure of the composite system.

In this paper, we chose Pt(111) as a non-ferromagnetic catalytic substrate to grow large G flakes with quasi-free-standing electronic structure.<sup>28</sup> We decided to use Fe as the intercalating agent because of its peculiar electrical and magnetic properties and the large knowledge accumulated by surface science studies on the FeO<sub>x</sub>/Pt(111) system.<sup>29,30,31,32,33</sup>

The electronic interactions induced by Fe intercalation are quite subtle and require the use of advanced investigation tools. Therefore, in the present work, photoemission from core-level, x-ray absorption near edge structure (XANES) and ARPES were carried out by synchrotron radiation and the results were interpreted with the assistance of density functional theory (DFT) calculations. However, in order to be correctly understood, the electronic structure information has to be combined with a precise picture of the morphology of the G lattice at the atomic scale. We therefore also performed STM experiments in order to disentangle intrinsic effects (electronic hybridization) from the role of structural defects, which may be present at the interface. Interestingly, the structure of the G layer is not modified by intercalation thanks to a possible epitaxial matching between Fe and Pt<sup>34</sup>. This suggests that this bimetallic system is an ideal trial ground to investigate selectively the electronic coupling between G and metals, ruling out other spurious effects.

The aim of our work is to study how Fe interacts with the G/Pt(111) system after *in-situ* ultra-high-vacuum (UHV) deposition, either at room (RT) or at high (T=600 K) temperature. In this manner, we obtained two different systems: supported Fe nanoparticles (NPs) (hereafter Fe/G/Pt(111)) and intercalated Fe layers (hereafter G/Fe/Pt(111)), respectively. In both cases, our experimental and theoretical data indicate a strong hybridization between the Fe layer and G, which has the notable effect of lifting the G  $\pi$  band spin degeneracy. Moreover, a study of the oxidation at RT of these interfaces is presented: we show that a reversible hybridization of G occurs in the case of Fe/G/Pt(111), whereas intercalated Fe in G/Fe/Pt(111) is unaffected by exposure to oxygen.<sup>35</sup> These data suggest that the G/Fe/Pt(111) system can be a good platform to grow arrays of intercalated ferromagnetic metallic islands that could be protected from air oxidation.

## Experimental section

A Pt(111) single crystal was cleaned by repeated cycles of sputtering (1.5 kV, 1x10<sup>-6</sup> mbar of Ar) and annealing at 1100 K; the surface cleanness was checked by photoemission and the morphology by low energy electron diffraction (LEED) and STM.

G was grown *in-situ* on Pt(111) by ethylene dosing, and Fe was deposited by *in-situ* physical vapor deposition (PVD); the Fe evaporator was calibrated based on the reconstructions of Fe<sub>x</sub>O<sub>y</sub> ultrathin films grown on Pt(111), at increasing Fe coverage. The Fe film was deposited at RT in UHV and post-oxidized in 1x10<sup>-6</sup> mbar of O<sub>2</sub> at 900 K.<sup>28,29</sup> The film growth was monitored by LEED and STM: the transition of LEED patterns between FeO and multi-layer Fe<sub>3</sub>O<sub>4</sub> ultrathin films occurs at 2 ML nominal FeO coverage, when STM also shows the onset of the growth of Fe<sub>3</sub>O<sub>4</sub> islands.<sup>36,37</sup> One ML of FeO corresponds to 2.16x10<sup>15</sup> Fe atoms/cm<sup>2</sup>. 1 ML Fe is defined as 2.60x10<sup>15</sup> Fe atoms/cm<sup>2</sup> considering its pseudomorphic growth on Pt(111).<sup>38</sup> XPS (x-ray photoemission spectroscopy) from core levels and XANES spectra were acquired at the BACH beamline at synchrotron ELETTRA (Trieste). Photoemission spectra from C 1s core levels were recorded with 550 eV photons, 20 eV pass energy and with an energy resolution of 130 meV. The XANES data of the Fe L<sub>2,3</sub>-edge were obtained in total electron yield or partial electron yield, with a linear horizontal polarization and an energy resolution of 160 meV.

The valence band (VB) structure was investigated by ARPES at the Spectromicroscopy beamline at synchrotron ELETTRA (Trieste), using 74 eV photons, 20 eV pass energy and with an energy resolution of 125 meV. The beam size was about 1  $\mu$ m. ARPES analyses were focused on the dispersion of the G  $\pi$  and  $\sigma$  bands from the  $\Gamma$  to K point of the first Brillouin zone. The investigated binding energy (BE) range was from 0 to 24 eV, which includes Pt 5d and Fe 3d bands.

The STM measurements were performed in a UHV multiscan lab from Omicron equipped with LEED optics, and a photoelectron spectrometer. STM images were acquired in constant current mode at RT with Pt/Ir tips cleaned by electron bombardment.

## Computational Methods

All calculations were performed using spin-polarized density functional theory (DFT), as implemented in the VASP code.<sup>39,40</sup> Projector augmented wave potentials<sup>41,42</sup> were used to describe the electron-ion interactions, and the generalized gradient approximation (GGA-PW91)<sup>43</sup> was used to describe the exchange-correlation functional. Van der Waals forces were included through the optB88-vdW functional using the vdW-DF approach.<sup>44,45,46</sup> The electron wave function was expanded using plane waves with an energy cutoff of 400 eV. The Pt(111) surface was modeled with a four layer periodic slab, with eight equivalent layers of vacuum separating successive slabs. A graphene-(2x2)/Pt(111)-( $\sqrt{3}\times\sqrt{3}$ )R30° surface unit cell, with 8 carbon atoms and three Pt atoms per layer, was used. This graphene-(2x2) phase is one of the most stable phases observed in experiments.<sup>47</sup> The graphene-(3x3)/Pt( $\sqrt{7}\times\sqrt{7}$ )R19° phase is another stable phase that was observed in our STM experiments (discussed later). We thus performed additional calculations using a larger graphene-(3x3)/Pt( $\sqrt{7}\times\sqrt{7}$ )R19° unit cell. These calculations show that the results obtained on the larger graphene-

$(3\times 3)/\text{Pt}(\sqrt{7}\times\sqrt{7})\text{R}19^\circ$  unit cell are similar to those of the smaller graphene $(2\times 2)/\text{Pt}(111)-(\sqrt{3}\times\sqrt{3})\text{R}30^\circ$  unit cell. The band structure of the larger graphene- $(3\times 3)/\text{Pt}(\sqrt{7}\times\sqrt{7})\text{R}19^\circ$  system is more difficult to visualize: there are more bands in the first Brillouin zone, making the highlights of  $C p_z$  and  $\text{Fe } 3d$  orbitals difficult to see. We thus, for clarity, only present our results for the smaller graphene- $(2\times 2)/\text{Pt}(111)-(\sqrt{3}\times\sqrt{3})\text{R}30^\circ$  unit cell.

For Fe adsorption or intercalation, three Fe atoms were introduced, corresponding to a coverage of one monolayer (ML). For FeO adsorption, a larger unit cell, graphene  $(4\times 2)/\text{Pt}(111)-(2\sqrt{3}\times\sqrt{3})$ , was used to account for the antiferromagnetic behavior of FeO. Six FeO clusters were adsorbed in each  $(2\sqrt{3}\times\sqrt{3})$  unit cell, corresponding to a coverage of one ML. For FeO, the DFT+U approach by Dudarev<sup>48</sup> was used to correct for the on-site Coulomb interaction between Fe  $3d$  orbitals, with parameters chosen so that  $U-J=3$  eV.<sup>49</sup>

The surface Brillouin zone (BZ) of  $\text{Pt}(111)-(\sqrt{3}\times\sqrt{3})$  was sampled using an  $(11\times 11\times 1)$  Monkhorst-Pack  $k$ -point mesh.<sup>50</sup> During optimization, the bottom two layers were fixed at the optimized bulk lattice constant of Pt, 3.99 Å, which is in good agreement with experimental values.<sup>51</sup> All structures were relaxed until the Hellmann-Feynman forces acting on atoms were less than 0.01 eV/Å. The dipole correction to the electrostatic potential was included.<sup>52</sup>

## Results and discussion

### G/Pt(111)

G was grown by the carbon segregation technique<sup>53</sup> by dosing 150 L of  $\text{C}_2\text{H}_4$  ( $6.5\times 10^{-7}$  mbar for 5 minutes) at 1000 K on Pt (111) and cooling down the crystal at 30 K/min. Following this procedure, high quality films were obtained, which show the typical Moiré-like  $\text{R}19^\circ$  LEED superstructure (Figure 1.a),<sup>53</sup> whereas STM images indicate also the presence of other superstructures (the higher corrugated islands in Figure 1.b). In general the mean size of rotationally different G domains is around 20-30 nm, but sometimes very large (>500 nm) single domains can be observed.

The G  $\text{R}30^\circ$  phase along with the  $\text{R } 19^\circ$  were observed by LEED but not with STM; however spectroscopic investigations are not very sensitive to the type of G reconstruction, so our DFT calculations are consistent with the experimentally-observed phase.

The G/Pt(111) system shows a sharp  $C 1s$  peak centered at a binding energy (BE) of 284.16 eV (Figure 2.a) that can be fitted by a single component characterized by a Doniach Sunjic line shape. The analysis of the ARPES data (Figure 3.a) indicates that the  $\pi$  band of G is scarcely interacting with the Pt  $5d$  states; around the K point, the  $\pi$  band of G displays a linear dispersion as in quasi-free-standing layer.<sup>54,55</sup> The Dirac point energy, extrapolated from the crossing of a linear extrapolation of the  $\pi$  band close to the K point (Figure 3.a), is slightly above the Fermi level (+ 0.2-0.3 eV), indicating that the G is slightly p-

doped by the Pt contact.<sup>28</sup> This is corroborated by our calculated band structures of G/Pt(111) shown in Figure 4, where a 0.55 eV downshift of the Fermi level with respect to the G conical point is found. The Fermi level shift results from the equilibration of the chemical potentials of G and Pt substrate,<sup>54,56</sup> though G is weakly physisorbed on Pt, with a calculated binding energy of -0.14 eV per two carbon atoms and a vertical distance of 3.41 Å above Pt within optB88-vdW. Indeed, a Bader charge analysis<sup>57</sup> shows that there is charge transfer (ca. 0.05 e) from G to the Pt substrate.

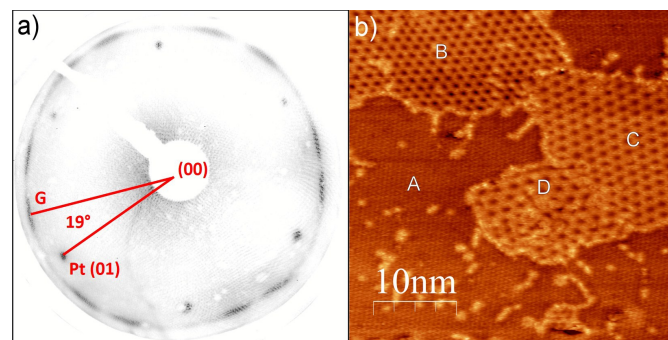


**Fig. 1** a) LEED pattern ( $E=55$  eV) and b) different 'flakes' of bare G/Pt(111) as shown by STM ( $V=-27$  mV;  $I=20.9$  nA), with typical 20-30 nm average size. The graphene flakes in the figure above show some of the possible rotational domains observed on Pt(111): A- $(3\times 3)$ , B- $(\sqrt{37}\times\sqrt{37})\text{R}21^\circ$ , C- $(\sqrt{61}\times\sqrt{61})\text{R}26^\circ$ , D- $(\sqrt{67}\times\sqrt{67})\text{R}12^\circ$ .

### In-situ iron deposition and intercalation

Fe was deposited *in-situ* by PVD at RT on G/Pt(111) to obtain Fe/G/Pt(111). For core-level photoemission experiments, an increasing amount of Fe was evaporated on the surface (0.5, 1 and 1.5 ML), whereas for ARPES experiments only the 1 ML coverage was chosen to avoid a strong attenuation of the G spectroscopic features. Figures 2.b,c,d show the evolution of the  $C 1s$  photoemission line as a function of the Fe coverage.

After a least square fit analysis, three different components were clearly identified: the peak at  $\text{BE}=284.16$  eV is due to the unperturbed  $\text{sp}^2$  atoms, whereas the two new components at 284.40 eV and 285 eV are associated with the formation of the Fe/G interface, as confirmed by the intensity increase as a function of metal deposition. The component at 284.40 eV is likely connected to  $C \text{sp}^2$  atoms underneath a metal island. The shift toward higher BE with respect to uncovered C atoms is the consequence of the strong cohesive energy between G and Fe.<sup>58</sup> Analogous to similar results reported in the literature for other metals,<sup>59,60</sup> the small component at 285 eV can be associated with a local rehybridization of G to  $\text{sp}^3$  carbon, also driven by the strong Fe-C interaction. From the absence of  $C 1s$  peak components at ca 283.2 eV (Figure 2.b-f) and from the Fe  $L_{2,3}$  XANES data (Figure 5.a,c), which indicate a zerovalent nature of Fe,<sup>61</sup> we can exclude the formation of iron carbides.

A Volmer-Weber (VW) type 3D island growth of Fe NPs is observed in Fe/G/Pt(111) at very low coverage ( $\sim 0.1$  ML) and RT, with a preferential nucleation at G domain boundaries and point defects (Figure 6.a,b,c).<sup>8</sup> The Fe NPs have a small size dispersion; they are typically round-shaped with a diameter of

2-3 nm (Figure 6.d) with an average thickness of several layers. This is very similar to previous results reported for the growth of Fe islands on G/Rh(111),<sup>8</sup> and other metal NPs on G/Ru(0001).<sup>62</sup> The VW-type 3D growth of Fe NPs on G is also confirmed by photoemission: the C 1s spectra (Figure 2.b-d) show that the component at 284.16 eV, pertaining to uncovered G on Pt(111), is visible even if the coverage exceeds 1 ML.

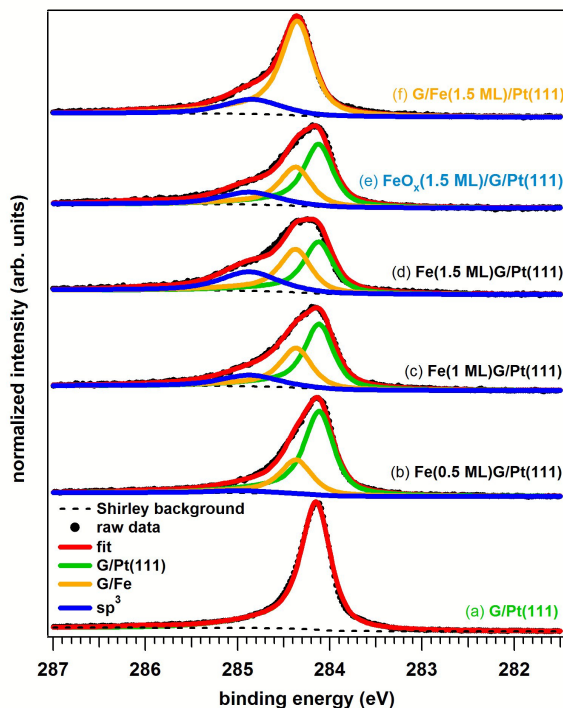


**Fig. 2** Normalized C 1s photoemission peaks (photon energy  $h\nu=550$  eV) of (a) G/Pt(111), (b) Fe(0.5ML)/G/Pt(111), (c) Fe(1.0ML)/G/Pt(111), (d) Fe(1.5ML)/G/Pt(111), (e) FeO<sub>x</sub>(1.5ML)/G/Pt(111) oxidized at RT, (f) G/Fe(1.5ML)/Pt(111) intercalated at 600 K.

The intercalated system, G/Fe/Pt(111), was obtained at high temperature, by depositing Fe on the G/Pt(111) system directly at 600 K or by post-annealing the Fe/G/Pt(111) system at 700 K for 5 minutes.<sup>63</sup> The relatively high temperature was necessary to obtain a flat Fe layer<sup>34</sup> and to intercalate G completely. Temperature and time were tuned to avoid the formation of a Pt/Fe alloy, however the possibility that a minor amount Fe migrates into the subsurface of Pt cannot be excluded. (See Electronic Supplementary Information for a detailed discussion about the alloy formation).

Two strong experimental evidences from STM and ARPES data demonstrate the intercalation process of Fe beneath G. The STM data reported in Figure 7 indicate that, after 0.3 ML Fe deposition at 600 K, Fe monolayer islands are formed on the Pt surface, which are covered by a continuous unperturbed layer of G. Moreover, at particular tunneling conditions the Moiré pattern visible on top of these islands is the same as that observed for G on Pt(111), however the bias dependence of the Moiré corrugation of adislands is different from the main terraces, indicating the presence of compositionally distinct interfaces with G in the two cases.

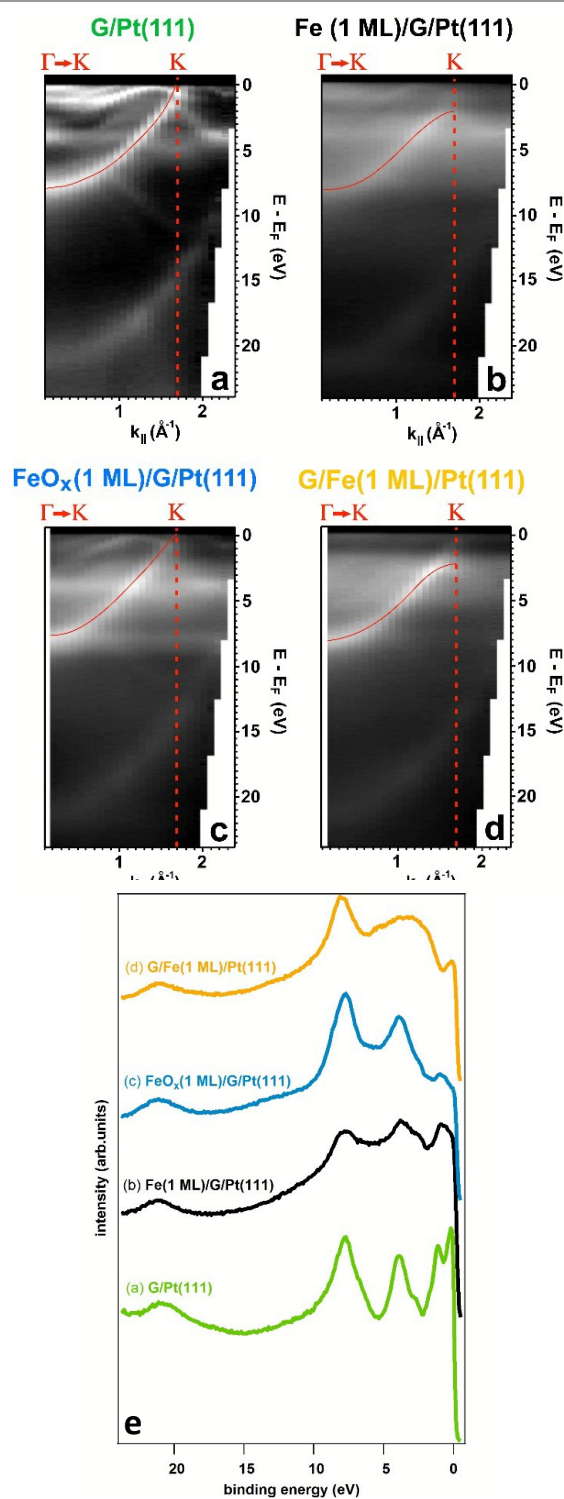


**Fig. 3** ARPES plot from  $\Gamma$  to K point of G first Brillouin zone obtained (photon energy  $h\nu=74$  eV) for (a) G/Pt(111) (b) Fe(1ML)/G/Pt(111), (c) FeO<sub>x</sub>(1ML)/G/Pt(111) oxidized at RT and (d) G/Fe(1ML)/Pt(111) intercalated at 600 K. Dashed red line are for the theoretical position of the K point in a free-standing G layer. (e) Valence band spectra acquired in  $\Gamma$ .

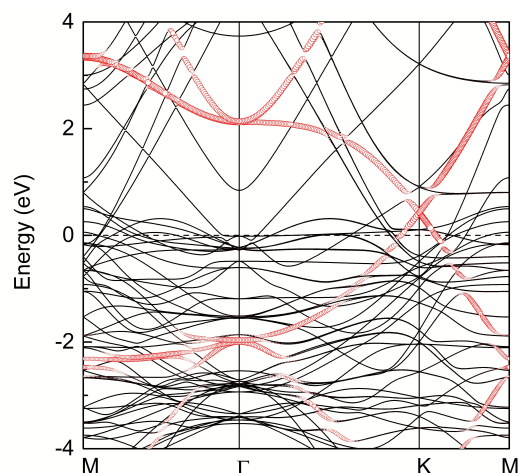


**Fig. 4** Band structure of graphene-(2×2)/Pt(111)-( $\sqrt{3}\times\sqrt{3}$ )R30°. The contributions of carbon  $2p_z$  orbitals are highlighted in red. A 0.55 eV downshift of the Fermi level with respect to the graphene conical point is observed at K. The Fermi level is set at zero.

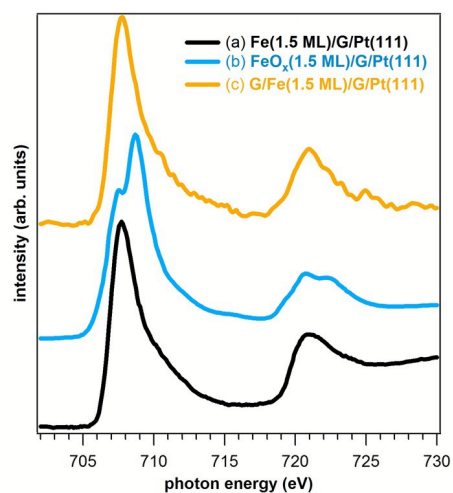


**Fig. 5** Fe  $L_{2,3}$  XANES data for (a) Fe(1.5ML)/G/Pt(111), (b) FeO<sub>x</sub>(1.5ML)/G/Pt(111) obtained after dosing 150 L of O<sub>2</sub> at RT and (c) G/Fe(1.5ML)/Pt(111) intercalated at 600 K.

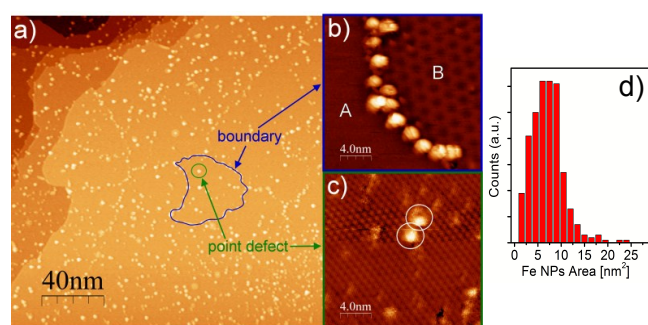


**Fig. 6:** (a) Large area STM view of low coverage Fe(0.1 ML)/G/Pt(111) system ( $V=1.5V$ ;  $I=0.3nA$ ) outlines 3D VW-type growth of Fe NPs at RT on pristine G/Pt(111) film, (b) STM ( $V=-0.69V$   $I=0.63$  nA) of Fe NPs nucleated at boundary of contiguous (3×3) (A) and ( $\sqrt{67}\times\sqrt{67}$ )R12° (B) G flakes, (c) STM ( $V=-65$  mV  $I=40$  nA) of Fe NPs pinned on point defects of a ( $\sqrt{37}\times\sqrt{37}$ )R21° G flake, (d) histogram of the Fe NPs areas.

This can be explained by the pseudomorphic growth of Fe islands on Pt(111),<sup>64,65</sup> which determines the same lattice mismatch at both G/Pt and G/Fe interfaces.

Differently to the growth of intercalated epitaxial islands underneath G grown on Rh(111) (G/Ni/Rh(111) and G/Fe/Rh(111)) where the local spatial variation of G-Rh(111) controls the size and shape of intercalated island,<sup>8</sup> the shape of the Fe NPs is random and there is not a significant size selection of the dimension, indicating that the interaction between G and the Pt substrate is scarce and does not hinder the atom diffusion below the G layer.

Interestingly, whereas in the Fe/G/Pt(111) system 3D Fe islands are observed, the intercalated Fe islands are flat. This is evident from the STM images and is also confirmed by the XPS data. In the G/Fe(1.5ML)/Pt(111) intercalated system, the peak at 284.16 eV, which is the fingerprint of G in contact with Pt(111), is completely suppressed (Figure 2.f). In the case of G/Fe/Pt(111), the residual presence of the 285 eV peak is probably due to the trapping of Fe into G defects. The photoemission data and STM therefore indicate that the intercalation is quantitative and leads to flat islands with an exclusive Fe/G interface. Comparing the distribution of the Fe islands in Figures 6.a and 7.a, we can deduce an easy diffusion of the Fe atoms underneath the G layer in order to form large islands, which is in contrast to the intercalation of Fe in G/Rh(111). This is caused by the different strength of the G-substrate interaction, which is larger for Rh(111) than for Pt(111). In the former, because of the presence of locally strong Rh-C bonds, the G layer limits atomic diffusion at the G/Rh interface, and the shape, orientation and size of the Fe islands is highly influenced. On the contrary, the carbon layer in G/Pt(111) is an adaptive cover that can be easily lifted to accommodate atom diffusion and the growth of large islands.

The relative intensity of the G bands and Fe  $3d$  states in the ARPES spectra is very informative. In the case of Fe(1ML)/G/Pt(111) (Figure 3.b), the G  $\pi$  band (c.a. 8.1 eV) is strongly attenuated by Fe, and its intensity in  $\Gamma$  is almost as strong as the metallic features at about 3 eV (Figure 3.b). On G/Fe(1ML)/Pt(111) (Figure 3.d), the G  $\pi$  band has a much higher relative intensity, showing an intensity comparable to the G/Pt(111) system (Figure 3.a), confirming the presence of G on the surface.

ARPES data also show major differences in the G band dispersion between G/Pt(111) and G/Fe interfaces. As mentioned before, in the G/Pt(111) case (Figure 3.a), the G  $\pi$  band displays a linear dispersion close to the K point as in quasi-free-standing layer. On the contrary, when G is in contact with Fe, either because it supports Fe NPs (in Fe/G/Pt(111), Figure 3.b), or as a consequence of the intercalation (in G/Fe/Pt(111), Figure 3.d), a relevant hybridization of its  $\pi$  band with Fe  $3d$  states can be observed.

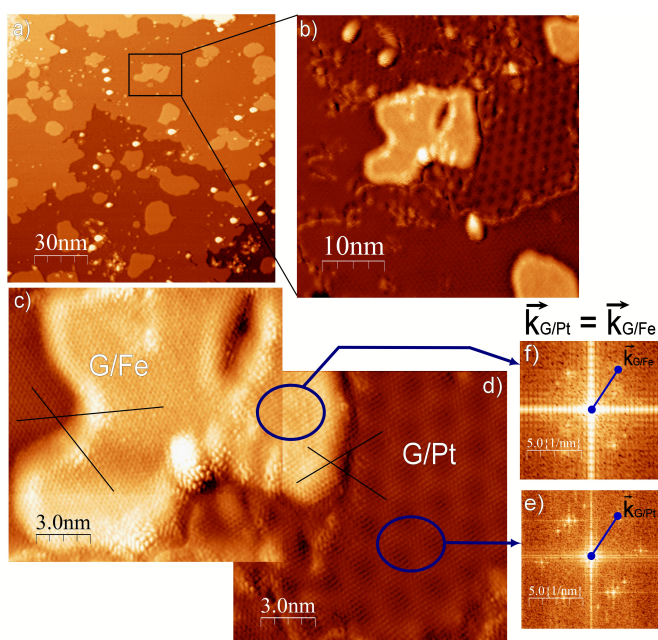


**Fig. 7:** (a) Large area STM view ( $V=-1.5\text{V}$   $I=0.3\text{ nA}$ ) of the intercalated G/Fe(0.3 ML)/Pt(111) system. Buried and 1 ML-thick Fe islands are observed, (b) Higher resolution detail ( $V=-28\text{ mV}$   $I=21.3\text{ nA}$ ) on a Fe island decorated by two contiguous G flakes with different epitaxy. (c) and (d) ( $V=-28\text{ mV}$   $I=34.6\text{ nA}$ ) show atomic lattice of G lying on Fe and Pt. Black lines are used to outline that the G film continues as an unperturbed lattice stack both at Fe/Pt(111) and Pt(111) interfaces. Variation in electronic Moiré contrast is observed in (d), when G is at the Fe interface. (e) is the FFT-STM of the G/Pt(111) region of d), while (f) is the FFT of the G/Fe/Pt(111) region: reciprocal lattice vectors  $\vec{k}_{\text{G/Pt}}$  and  $\vec{k}_{\text{G/Fe}}$  of graphene are actually the same ( $k=4.13\pm 0.01\text{ nm}^{-1}$ ), corresponding to 2.42–2.43 Å.

The experimental data show that the G electronic structure is strongly modified by the Fe interface: from the  $\Gamma$  to K point of the BZ, the dispersion of the  $\pi$  band is very similar to the G/Pt(111) case until the band crosses the energy range of the Fe 3d levels (4 eV). Starting from this point, the band deviates from the linear dispersion typically observed around the K point, bending and remaining pinned at about 2.4 eV below the Fermi level. Moreover, at the  $\Gamma$  point, a small shift towards higher BE (about 0.2 eV with respect to G/Pt(111)) of both the  $\pi$  and  $\sigma$  bands (Figure 3.e) can be noticed, even if in this energy range there is not a direct overlap with the Fe 3d states. Similar features are reported in the literature for G interacting with other non-noble *d*-metals, such as Ni(111), and are connected to an overall n-doping of the G layer.<sup>21,66,67,68</sup>

To understand the electronic structures of the Fe/G/Pt(111) and G/Fe/Pt(111) systems, we calculated Fe adsorption/intercalation on/in G/Pt at Fe coverage of one ML. Figure 8.a shows the optimized structure of Fe(1ML)/G/Pt, where the Fe monolayer is 2.3 Å above G. The adsorption of one ML Fe moves the G layer ca. 0.2 Å closer to the Pt substrate, resulting in a vertical distance of 3.19 Å between G and Pt, compared with 3.41 Å found in G/Pt. Using atomic Fe energy as a reference, the calculated binding energy of one ML Fe adsorbed on G/Pt(111) is -3.17 eV per Fe atom. Bader charge analysis indicates that one ML Fe donates a total of 0.49 e, 0.36 e to graphene and 0.13 e to the Pt substrate. The spin-resolved band structures of

Fe(1ML)/G/Pt(111) are plotted in Figure 9, with the contributions of carbon  $2p_z$  and Fe 3d states highlighted. We first notice that due to the interaction with Fe states, the G  $\pi$ -bands are non-degenerate within two spin channels. Furthermore, the linear dispersion near the K point shown in the band structures of G/Pt without Fe is perturbed due to the hybridization between carbon  $2p_z$  and Fe 3d orbitals (cf. Figure 9.a and c, or b and d). The Dirac point is roughly 0.4 and 1.7 eV below the Fermi level in the majority and minority spin channels, respectively. The downshift (upshift) of the Dirac point (Fermi level) is consistent with the Bader charge analysis discussed above.

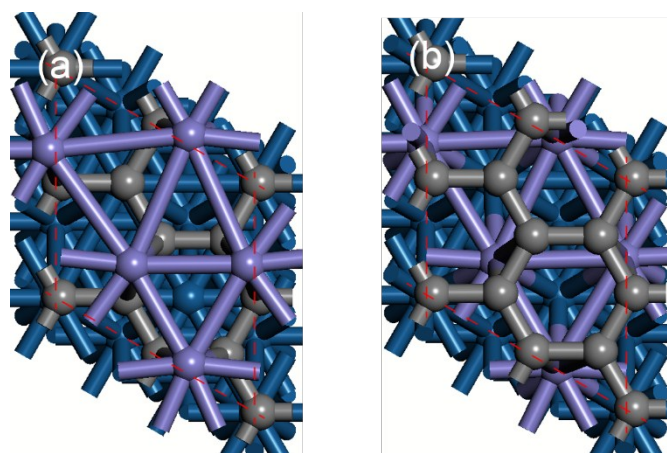


**Fig. 8:** Optimized structure of graphene/Pt(111) with one monolayer Fe (a) adsorbed on top of graphene, and (b) intercalated between graphene and Pt(111) substrate. Gray, purple, and dark blue spheres indicate C, Fe, and Pt atoms, respectively.

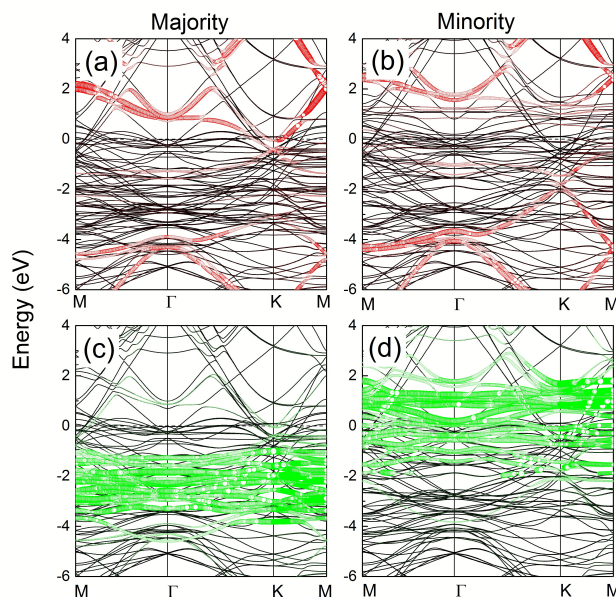


**Fig. 9:** Band structures of one ML Fe adsorbed on G/Pt(111). (a) Majority spin and (b) minority spin band structures with the contributions of carbon  $2p_z$  states are highlighted in red. The contributions of Fe 3d states to (c) majority and (d) minority spin band structures are highlighted in green. The Fermi level is set at zero.

We next describe Fe intercalation between G and Pt(111). Figure 8.b shows the top view of the atomic structure of G/Fe(1 ML)/Pt(111). In the optimized structure, the one ML Fe is 2.0 Å above the Pt substrate, while graphene is 2.1 Å above the Fe layer. Remarkably, our calculations show that the intercalated system G/Fe(1ML)/Pt(111) is -1.82 eV per Fe atom more stable than the adsorbed system Fe(1ML)/G/Pt(111), primarily due to the strong interaction between Fe and Pt substrate. This can be partly understood from Bader charge analysis: the intercalated one ML Fe donates 1.44 e; Pt accepts 0.84 e, and the remaining 0.6 e is donated to G.

The band structures of the intercalated system G/Fe(1ML)/Pt(111) are shown in Figure 10. The contributions of carbon  $2p_z$  and Fe  $3d$  states are highlighted in red and green, respectively. Similarly to the case of the adsorbed system, the graphene  $\pi$ -bands of the Fe intercalated system are non-degenerate within two spin channels: the Dirac point is roughly at 0.4 and 2.3 eV below the Fermi level in the majority and minority spin channels, respectively. We note that the downshift of the Dirac point at the minority spin channel (Figure 10.b) in the intercalated system is larger than the corresponding downshift in the adsorbed system (Figure 9.b). This can be explained by the fact that more electrons are transferred to graphene in the intercalated system than in the adsorbed system (Bader charge 0.6 e vs 0.36 e).

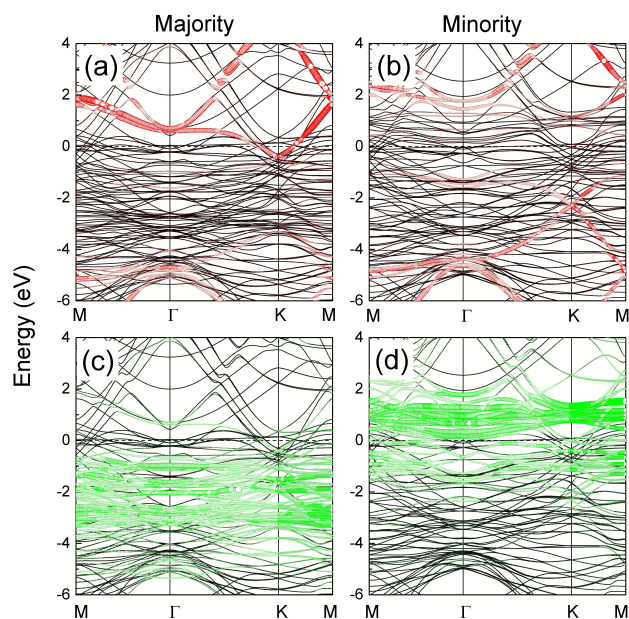


**Fig. 10.** Band structures of the intercalated system G/Fe(1ML)/Pt(111). (a) Majority spin and (b) minority spin band structures with the contributions of carbon  $2p_z$  states are highlighted in red. The contributions of Fe  $3d$  states to (c) majority and (d) minority spin band structures are highlighted in green. The Fermi level is set at zero.

In Figure 11, we compare the projected density of states on C  $2p$ , Fe  $3d$ , and Pt  $5d$  of Fe(1ML)/G/Pt(111) and G/Fe(1ML)/Pt(111). As shown, in the intercalated system, the Fe  $3d$  orbitals in the majority spin are broadened due to the interaction with Pt  $5d$  orbitals. This is also clearly shown in the

band structures with Fe  $3d$  contributions highlighted, Figure 10.c.

To compare the ARPES map of the flat intercalated layer, Figure 3.d, with the calculated band structure, we show in Figure 12 an enlargement of the ARPES spectra of G/Fe(1ML)/Pt(111) close to the G K point. The band splits in two components at about 3 eV. One branch continues up to 0.6 eV and the other remains pinned at 2.4 eV. This is in excellent agreement with the calculated majority and minority spin band structures of G/Fe(1 ML)/Pt(111) shown in Figure 10.a and b. An alternative interpretation of the  $\pi$  band splitting reported in Figure 12 could be that a minority part of G remains in contact with Pt either because of an insufficient iron deposition or as a consequence of the presence of a Pt skin due to the formation of a PtFe alloy (see below and ESI). This hypothesis however would require that the doping level of the G/Pt(111) or G/Pt<sub>skin</sub>FePt is profoundly modified with respect to normal conditions (0-0.3 eV p-doping), maybe by the interaction with surrounding G/Fe(1 ML)/Pt(111) domains.

It is worth mentioning that for Fe/G/Pt(111), direct comparison of the experimental data with the calculated band structures is rather difficult because 3D NPs are formed when 1 ML of Fe is deposited at RT. Some G/Pt(111) is likely not covered by Fe and can be sampled by photoemission, making the final ARPES map a combination of Fe/G/Pt(111) and G/Pt(111). Furthermore, the Fe band structures can be modified by the size of the Fe NPs and consequently be different from one flat monolayer placed above G, as assumed in the calculations.

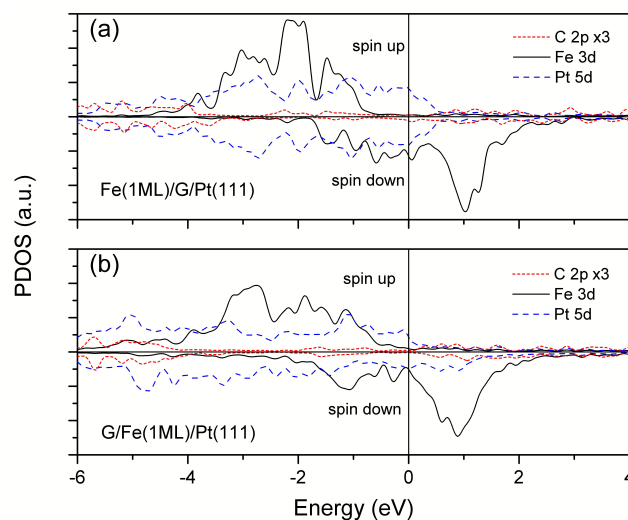


**Fig. 11.** Projected density of states of (a) Fe(1 ML)/G/Pt(111), and (b) G/Fe(1 ML)/Pt(111) on C  $2p$ , Fe  $3d$ , and Pt  $5d$  orbitals. The Fermi level is set at zero.

To examine the effect of Fe adsorption and intercalation on the C  $1s$  core level, we calculated the core-level shift in the final state approximation using the method of Köhler and Kresse,<sup>69</sup>

$$E_{CLS} = [E_{Fe/G/Pt(111)}(n_c - 1) - E_{Fe/G/Pt(111)}(n_c)] - [E_{G/Pt(111)}(n_c - 1) - E_{G/Pt(111)}(n_c)]$$

where  $E_i$  is the total energy of configuration  $i$ , and  $E(n_c)$  and  $E(n_c-1)$  are the total energies of the ground state and excited state, respectively, of a carbon  $1s$  electron.

Our DFT results show that the C  $1s$  core level in the Fe(1ML)/G/Pt(111) system shifts 0.22 eV to higher BE with respect to the C  $1s$  core level in G/Pt(111). This is in excellent agreement with the XPS experimental data on Fe/G/Pt(111), where a core level shift of 0.24 eV was observed (from 284.16 to 284.40 eV). For G/Fe(1ML)/Pt(111) intercalated system, the calculated C  $1s$  core level shift is 0.60 eV to higher BE using C  $1s$  core level in G/Pt(111) as a reference. We note that the core level shift depends on Fe coverage. At Fe coverage of 1/3 ML, i.e., one Fe atom adsorbed or interacted on/in graphene-(2×2)/Pt(111)- $\sqrt{3}\times\sqrt{3}$ R30° unit cell, the calculated C  $1s$  core level shift is 0.33 and 0.34 eV to higher BE for Fe(1/3 ML)/G/Pt(111) and G/Fe(1/3 ML)/Pt(111), respectively. The smaller shift observed experimentally for G/Fe(1.5ML)/Pt(111) could be caused by the partial alloying of the Fe layer with the platinum substrate.

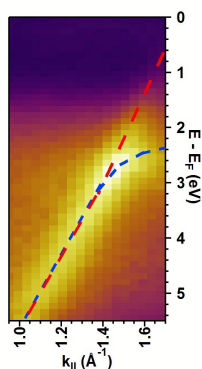


**Fig. 12:** Enlarged view of ARPES of G/Fe(1 ML)/Pt(111) close to the G K point. Underlined with dashed red line spin majority band and in blue spin minority band.

Actually, additional calculations for 1 ML Fe adsorbed on the Pt(111) surface, and for the incorporation of 1 ML of Fe atoms below the first and second Pt layer, all in the absence of G, provide formation energies of -4.89, -5.81, -5.61 eV, respectively. Although the models tested do not mix Pt and Fe within a given slab layer, these results indicate that Fe could easily alloy with the Pt substrate. Therefore, we used the most stable alloy, i.e. Pt(1ML)/Fe(1ML)/Pt(111), to support a G layer. It turns out that the G/Pt(1ML)/Fe(1ML)/Pt(111) (see fig. S2) system is 2.26 eV (i.e. -0.75 eV /Fe atoms) more stable than G/Fe(1ML)/Pt(111). Interestingly, for this system the calculated band structure of G (see ESI Fig. S3) is very similar to the simple G/Pt(111) interface: the Dirac energy is located at 0.3 eV above the Fermi level and the  $\pi$  band is spin degenerate and displays a linear dispersion around the K point. These results indicate that even a single layer of Pt is sufficient to restore the non-interacting regime. Since the experimental ARPES data show a profound modification of the pristine G band structure and are compatible only with the features of G/Fe(1ML)/Pt(111), we can conclude that the formation of the

alloy, even if thermodynamically favoured, is prevented by kinetic factors.

### Iron oxidation at room temperature

We carried out a spectroscopic investigation of the Fe(1.5ML)/G/Pt(111) system after dosing molecular oxygen ( $6.5\times 10^{-7}$  mbar, 150 L at RT) in order to oxidize the outer shell of the Fe islands (hereafter FeO<sub>x</sub>(1.5ML)/G/Pt(111)). The XANES measurements (Figure 5.b) indicate a clear modification of the Fe L<sub>2,3</sub>-edges, which is characterized by a complex line shape that can be due to the overlap of two components, one coming from a residual metal phase and another one related to non stoichiometric iron oxides.<sup>70</sup>

Because of the Fe oxidation, the 284.4 eV component of the C  $1s$  photoemission line of the Fe(1.5ML)/G/Pt(111) system decreases (Figure 2.e), whereas the peak at 284.16 eV, assigned to G/Pt(111), becomes more intense, reaching almost the same relative intensity observed for Fe(0.5ML)/G/Pt(111) (Figure 2.b). Surprisingly, the component at c.a. 285 eV is also strongly suppressed after oxidation, demonstrating that the local C  $sp^3$  hybridization induced by Fe is reversible. The remaining peaks at 284.4 eV and 285 eV can be related to the metallic Fe/G interface, persisting in the lower inner portion of the islands.

The STM images of the oxidized surface are of low quality, likely due to the presence of residual mobile oxygen species (see Figure 13) and for the amorphous structure of FeO<sub>x</sub> NPs synthesized at RT that probably also causes the broad features at about 4.5 and 8 eV in the valence band spectrum (Figure 3.c), which do not show any energy dependence on  $k$  vector. Moreover, it can be seen that the morphology of the Fe NPs does not change significantly, and is characterized only by a small increment of the corrugation.

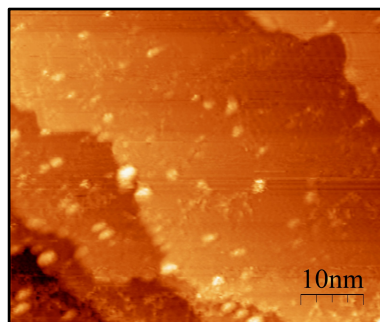


**Fig. 13:** STM images of the Fe(1.5ML)/G/Pt(111) system after dosing molecular oxygen ( $6.5\times 10^{-7}$  mbar, 150 L at RT).

The ARPES measurements taken after dosing 150 L O<sub>2</sub> on Fe(1 ML)/G/Pt(111) confirm the absence of any interaction between the FeO<sub>x</sub> layer and G, as evidenced by the complete recovery of the G  $\pi$  band, which is no longer hybridized with the Fe  $3d$  states (Figure 3.c). The overall G electronic band structure is very similar to the G/Pt(111) case (Figure 3.a). Finally, at the  $\Gamma$  point also the small shift towards higher BE observed for G/Fe interface disappears.

To illustrate the effect of the oxidation of Fe on G, we calculated the FeO adsorption on G/Pt(111) using a FeO(1

ML)/G(4×2)/Pt(2√3×√3) unit cell. After geometry optimization, the graphene is 3.43 Å above the Pt surface, and the FeO monolayer is located 3.84 Å above the graphene layer. Bader charge analysis shows that essentially no charge is transferred between FeO and G. This can be understood by the presence of the more electronegative O, which acts as an electron acceptor for the Fe donors and inhibits charge transfer from Fe to G. Considering the negligible interaction between FeO monolayer and G, the similarity of G band structures of FeO<sub>x</sub>(1ML)/G/Pt(111) and that of G/Pt(111) observed in experimental ARPES is expected.

Rather interestingly, any attempt to oxidize the G/Fe/Pt(111) system dosing the same amount of O<sub>2</sub> at RT was unsuccessful. Even when using a ten times higher oxygen dosage or direct air exposure we did not observe any iron oxidation. Further studies will be performed dosing oxygen at high temperature to exploit the gas intercalation;<sup>14,71</sup> however, the observed oxidation protection<sup>35</sup> of the Fe intercalated islands is a crucial finding for future spintronics devices.

## Conclusions

In this paper the interaction between a quasi-free-standing G layer, grown on Pt(111), and iron was studied. We demonstrated that when iron is deposited on G at RT it forms NPs that aggregate on G grain boundaries and point defects. On the contrary, if Fe is deposited on the substrate Pt(111) at 600 K, it intercalates beneath G, creating monolayer flat islands. G displays a perfect carpeting mode on the Fe intercalated island, and the carbon sp<sup>2</sup> lattice goes continuously from above the Fe intercalated islands down to the Pt(111) substrate. Photoemission from C 1s core level shows that the C 1s peak shifts to higher BE when Fe is deposited atop or intercalated beneath G. The C 1s core level shift was rationalized by charge transfer analysis and the core level shift calculations in late state approximation. The hybridization between Fe 3d states and G π band was visualized experimentally using ARPES, and demonstrated theoretically using band structures and projected density of states. We demonstrated that Fe NPs deposited above G can be easily oxidized, and in this case both the charge transfer and the hybridization cease. Conversely, Fe is well protected from the oxidation if it is intercalated beneath G. Remarkably, our DFT calculations show that the Fe contact lifts G spin degeneracy, inducing a clear split in the C 2p<sub>z</sub> band. Experimentally this is visible in the ARPES map of G/Fe(1 ML)/Pt(111), confirming the possibility to induce magnetism in monolayer G in contact with a monolayer of ferromagnetic material. Moreover, theoretical calculations indicate that the introduction a single Pt layer between G and Fe is sufficient to recover the electronic properties of self-standing G.

To summarize, the system G/Fe/Pt(111) is a strong candidate to study G magnetism in 2D devices for three principal reasons:

1. G sp<sup>2</sup> lattice homogeneously covers the Fe intercalated islands without inducing structural defects that could induce spurious magnetism;<sup>72</sup>

2. even if G is in contact with only one layer of ferromagnetic metal its spin degeneracy is removed therefore this system represents a suitable platform for realizing spin-filtering junctions;
3. intercalated Fe islands are efficiently protected by G from oxidation, which is a fundamental requirement for the development of practical devices.

## Acknowledgements

M.F. acknowledges Fondazione Cariparo for financial support. This work was supported by the Italian MIUR through the national grant Futuro in Ricerca 2012 RBFR128BEC “Beyond graphene: tailored C-layers for novel catalytic materials and green chemistry” and by the University of Padova funded project: CPDA128318/12 “Study of the catalytic activity of complex graphene nanoarchitectures from ideal to real conditions”.

Work at UW-Madison was partially supported by DOE-BES, Division of Chemical Sciences (grant DE-FG02-05ER15731) and by the Air Force Office of Scientific Research under a Basic Research Initiative grant (AFOSR FA9550-12-1-0481). The computational work was performed in part using supercomputing resources from the following institutions: the EMSL, a national scientific user facility at the Pacific Northwest National Laboratory (PNNL); the Center for Nanoscale Materials (CNM) at the Argonne National Laboratory (ANL); the National Energy Research Scientific Computing Center (NERSC); and the DoD High Performance Computing Modernization Program at the US Air Force Research Laboratory DoD Supercomputing Resource Center (AFRL DSRC), the US Army Engineer Research and Development Center (ERDC), and the Navy DoD Supercomputing Resource Center (Navy DSRC). The EMSL is sponsored by the Department of Energy’s Office of Biological and Environmental Research located at PNNL. The CNM and the NERSC are supported by the US Department of Energy, Office of Science, under Contracts DE-AC02-06CH11357, and DE-AC02-05CH11231, respectively.

## Author contributions

MC participated in all the experimental works except for the STM; GP and LR performed the spin polarized DFT calculations; EC carried out the STM investigation; LA and MC have done preliminary experiments in XPS-TPD home-lab setup; MC, LA, IP, SN, EM, FB were involved in the HR core level XPS and NEXFAS measurements at Bach beamline at Elettra; MC, AB and MF carried out the ARPES experiments at Spectromicroscopy beamline at Elettra; LG, SA, MM and GG drafted the paper and coordinated the work.

## Notes and references

<sup>a</sup> Department of Chemical Sciences, University of Padova, via Marzolo 1, I-35131 Padova, Italy; email: stefano.agnoli@unipd.it

<sup>b</sup> Department of Chemical and Biological Engineering, University of Wisconsin-Madison, 1415 Engineering Drive, Madison, WI 53706, USA.

<sup>c</sup> Interdisciplinary Laboratories for Advanced Materials Physics (i-LAMP) and Dipartimento di Matematica e Fisica, Università Cattolica, via dei Musei 41, I-25121 Brescia, Italy.

<sup>d</sup> Sincrotrone Trieste S.C.p.A., Area Science Park-Basovizza, Strada Statale 14 Km 163.5, I-34149 Trieste, Italy.

<sup>e</sup> Istituto Officina dei Materiali (IOM)-CNR, Laboratorio TASC, Area Science Park-Basovizza, Strada Statale 14 Km 163.5, I-34149 Trieste, Italy.

Electronic Supplementary Information (ESI) available:

- 1 G. Eda, G. Fanchini, and M. Chhowalla, *Nat. Nanotechnol.*, 2008, **3**, 270.
- 2 K. S. Novoselov, V. I. Fal'ko, L. Colombo, P. R. Gellert, M. G. Schwab and K. Kim, *Nature*, 2012, **490**, 192.
- 3 E. J. H. Lee, K. Balasubramanian, R. T. Weitz, M. Burghard and K. Kern, *Nat. Nanotechnol.*, 2008, **3**, 486.
- 4 N. Tombros, C. Jozsa, M. Popinciuc, H.T. Jonkman and B. J. Van Wees, *Nature*, 2007, **448**, 571.
- 5 P. Seneor, B. Dlubak, M. Martin, A. Anane, H. Jaffres and A. Fert, *MRS Bulletin*, 2012, **37**, 1245.
- 6 A. M. Shikin, G. V. Prudnikova, V. K. Adamchuk, F. Moresco and K. Rieder, *Phys. Rev. B*, 2000, **62**, 13202.
- 7 Y. S. Dedkov, A. M. Shikin, V. K. Adamchuk, S. L. Molodtsov, C. Laubschat, A. Bauer and G. Kaindl, *Phys. Rev.*, 2001, **64**, 0354051.
- 8 M. Sicot, P. Leicht, A. Zusan, S. Bouvron, O. Zander, M. Weser, Y. S. Dedkov, K. Horn and M. Fonin, *ACS Nano*, 2012, **6**, 151.
- 9 R. Addou, A. Dahal and M. Batzill, *Surf. Sci.*, 2012, **606**, 1108.
- 10 A. Nagashima, N. Tejima and C. Oshima, *Phys. Rev. B*, 1994, **50**, 17487.
- 11 M. Gyamfi, T. Eelbo, M. Wasniowska and R. Wiesendanger, *Phys. Rev. B*, 2012, **85**, 205434.
- 12 Y. Cui, J. Gao, L. Jin, J. Zhao, D. Tan, Q. Fu and X. Bao, *Nano Res.* 2012, **5**, 352.
- 13 P. Sutter, J. T. Sadowski, and E. A. Sutter, *J. Am. Chem. Soc.*, 2010, **132**, 8175.
- 14 R. Lariciprete, S. Ulstrup, P. Lacovig, M. Dalmiglio, M. Bianchi, F. Mazzola, L. Hornekær, F. Orlando, A. Baraldi, P. Hofmann and S. Lizzit, *ACS Nano*, 2012, **6**, 9551.
- 15 N. A. Vinogradov, K. Schulte, M. L. Ng, A. Mikkelsen, E. Lundgren, N. Martensson and A. B. Preobrajenski, *J. Phys. Chem. C*, 2011, **115**, 9568.
- 16 Y. Zhang, Q. Fu, Y. Cui, R. Mu, L. Jin, and X. Bao, *Phys. Chem. Chem. Phys.*, 2013, **15**, 19042
- 17 R. Mu, Q. Fu, L. Jin, L. Yu, G. Fang, D. Tan and X. Bao, *Angew. Chem.*, 2012, **51**, 4856.
- 18 L. Jin, Q. Fu, A. Dong, Y. Ning, Z. Wang, H. Bluhm, X. Bao *J. Phys. Chem C*, 2014 **118**, 12391
- 19 M. Weser, Y. Rehder, K. Horn, M. Sicot, M. Fonin, A. B. Preobrajenski, E. N. Voloshina, E. Goering, Y. S. Dedkov, *Appl. Phys. Lett.*, 2009, **96**, 012504.
- 20 Y. S. Dedkov and M. Fonin, *New J. Phys.*, 2010, **12**, 125004.
- 21 E. N. Voloshina, A. Generalov, M. Weser, S. Böttcher, K. Horn and Y. S. Dedkov, *New J. Phys.*, 2011, **13**, 113028.
- 22 M. Weser, E. N. Voloshina, K. Horn and Y. S. Dedkov, *Phys. Chem. Chem. Phys.*, 2011, **13**, 7534.
- 23 S. J. Sung, J. W. Yang, P. R. Lee, J. G. Kim, M. T. Ryu, H. M. Park, G. Lee, C. C. Hwang, K. S. Kim, J. S. Kim and J. W. Chung, *Nanoscale*, 2014, **6**, 3824.
- 24 V. M. Karpan, P. A. Khomyakov, A. A. Starikov, G. Giovannetti, M. Zwierzycki, M. Talanana, G. Brocks, J. van den Brink, and P. J. Kelly, *Phys. Rev. B*, 2008, **78**, 195419
- 25 R. Decker, J. Brede, N. Atodiresei, V. Caciuc, S. Blügel, and R. Wiesendanger, *Phys. Rev. B*, 2013, **87**, 041403(R).
- 26 K. Gotterbarm, W. Zhao, O. Höfert, C. Gleichweit, C. Papp and H.-P. Steinrück, *Phys. Chem. Chem. Phys.*, 2013, **15**, 19625
- 27 Y. Murata, E. Starodub, B. B. Kappes, C. V. Ciobanu, N. C. Bartelt, K. F. McCarty and S. Kodambaka *Appl. Phys. Lett.*, 2010, **97**, 143114.
- 28 P. Sutter, J. T. Sadowski and E. Sutter, *Phys. Rev. B*, 2009, **80**, 245411.
- 29 N. Spiridis, D. Wilgocka-Alęzak, K. Freindl, B. Figarska, T. Giela, E. Młyńczak, B. Strzelczyk, and M. Zając, J. Korecki, *Phys. Rev. B*, 2012, **85**, 075436.
- 30 L. Giordano, M. Lewandowski, I. M. N. Groot, Y. Sun, J. Goniakowski, C. Noguera, S. Shaikhutdinov, G. Pacchioni and H.-J. Freund, *J. Phys. Chem. C*, 2010, **114**, 21504.
- 31 L. Giordano, G. Pacchioni, J. Goniakowski, N. Nilius, E. D. L. Rienks and H.-J. Freund, *Phys. Rev. Lett.*, 2008, **101**, 026102.
- 32 L. R. Merte, G. Peng, R. Bechstein, F. Rieboldt, C. A. Farberow, L. C. Grabow, W. Kudernatsh, S. Wendt, E. Lægsgaard, M. Mavrikakis and F. Besenbacher, *Science*, 2012, **336**, 889.
- 33 L. R. Merte, R. Bechstein, G. Peng, F. Rieboldt, C. A. Farberow, H. Zeuthen, J. Knudsen, E. Lægsgaard, S. Wendt, M. Mavrikakis, F. Besenbacher, *Nat. Commun.*, 2014, **5**, 4193
- 34 T. Ma, Q. Fu, Y. Cui, Z. Zhang, Z. Wang, D. Tan and X. Bao, *Chin. J. Catal.*, 2010, **31**, 24.
- 35 Y. S. Dedkov, M. Fonin, U. Rüdiger and C. Laubschat, *Appl. Phys. Lett.*, 2008, **93**, 022509.
- 36 Y. J. Kim, C. Westphal, R. X. Ynzunza, Z. Wang, H. C. Galloway, M. Salmeron, M. A. Van Hove and C. S. Fadley, *Surf. Sci.*, 1998, **416**, 68.
- 37 M. Ritter, W. Ranke, W. and W. Weiss, *Phys. Rev. B*, 1988, **57**, 7240.
- 38 D. I. Jerdev and B. E. Koel, *Surf. Sci.*, 2002, **513**, L391.
- 39 G. Kresse and J. Furthmüller, *Phys. Rev. B*, 1996, **54**, 11169.
- 40 G. Kresse and J. Furthmüller, *Comput. Mat. Sci.*, 1996, **6**, 15.
- 41 P. E. Blöchl, *Phys. Rev. B*, 1994, **50**, 17953.
- 42 G. Kresse, and D. Joubert, *Phys. Rev. B*, 1999, **59**, 1758.
- 43 J. P. Perdew and Y. Wang, *Phys. Rev. B*, 1992, **45**, 13244.
- 44 J. Klimes, D. R. Bowler and A. Michealides, *J. Phys.: Condens. Matter*, 2010, **22**, 022201.
- 45 J. Klimes, D. R. Bowler, and A. Michaelides, *Phys. Rev. B*, 2011, **83**, 195131.
- 46 M. Dion, H. Rydberg, E. Schröder, D. C. Langreth, and B. I. Lundqvist, *Phys. Rev. Lett.*, 2004, **92**, 246401.
- 47 P. Merino, M. Švec, A. L. Pinardi, G. Otero and J. A. Martín-Gago, *ACS Nano*, 2011, **5**, 5627.

- 48 S.L. Durarev, G.A. Botton, S.Y. Savrasov, C.J. Humphreys, A.P. Sutton, *Phys. Rev. B*, 1998, **57**, 1505.
- 49 L. R. Merte, L. C. Grabow, G. Peng, J. Knudsen, H. Zeuthen, W. Kudernatsch, S. Porsgaard, E. Lægsgaard, M. Mavrikakis and F. Besenbacher, *J. Phys. Chem. C*, 2011, **115**, 2089.
- 50 H. J. Monkhorst, and J. D. Pack, *Phys. Rev. B*, 1976, **13**, 5188.
- 51 *CRC Handbook of Chemistry and Physics, 94th Edition* (ed William M. Haynes) (CRC Press/Taylor and Francis, Boca Raton, FL, 2014).
- 52 J. Neugebauer, and M. Scheffler, *Phys. Rev. B*, 1992, **46**, 16067.
- 53 M. Gao, Y. Pan, L. Huang, H. Hu, L. Z. Zhang, H. M. Guo, S. X. Du and H.-J. Gao, *Appl. Phys. Lett.*, 2011, **98**, 033101.
- 54 G. Giovannetti, P. A. Khomyakov, G. Brocks, V. M. Karpan, J. Van Den Brink, and P. J. Kelly, *Phys. Rev. Lett.*, 2008, **101**, 026803.
- 55 A. Politano, A. R. Marino, V. Formoso, and G. Chiarello, *Carbon*, 2012, **50**, 734.
- 56 P. A. Khomyakov, G. Giovannetti, P. C. Rusu, G. Brocks, J. Van der Brink and P. J. Kelly, *Phys. Rev. B*, 2009, **79**, 195425.
- 57 G. Henkelman, A. Arnaldsson, H. Jonsson, *Comput. Mater. Sci.*, 2006, **36**, 354.
- 58 D. Haberer, D. V. Vyalikh, S. Taioli, B. Dora, M. Farjam, J. Fink, D. Marchenko, T. Pichler, K. Ziegler, S. Simonucci, M. S. Dresselhaus, M. Knupfer, B. Büchner and A. Grüneis, *Nano Lett.*, 2010, **10**, 3360.
- 59 J. Knudsen, P. J. Feibelman, T. Gerber, E. Grånäs, K. Schulte, P. Stratmann, J. N. Andersen and T. Michely, *Phys. Rev. B*, 2012, **85**, 035407.
- 60 P. J. Feibelman, *Phys. Rev. B*, 2008, **77**, 165419.
- 61 J. Gao, J. Zhong, L. Bai, J. Liu, G. Zhao, and X. Sun, *Sci. Rep.*, 2014, **4**, 3606.
- 62 Z. Zhou, F. Gao, and D. W. Goodman, *Surf. Sci.*, 2010, **604**, L31.
- 63 M. Cattelan, E. Cavaliere, L. Artiglia, L. Gavioli, S. Agnoli and G. Granozzi, *Surf. Sci.*, doi:10.1016/j.susc.2014.11.017.
- 64 D. I. Jerdev and B. E. Koel, *Surf. Sci.*, 2002, **513**, L391.
- 65 D. Repetto, T. Y. Lee, S. Rusponi, J. Honolka, K. Kuhnke, V. Sessi, U. Starke, H. Brune, P. Gambardella, C. Carbone, A. Enders and K. Kern, *Phys. Rev. B*, 2006, **74**, 054408.
- 66 A. Dahal, M. Batzill, *Nanoscale*, 2014, **6**, 2548.
- 67 A. Varykhalov, J. Sánchez-Barriga, A. M. Shikin, C. Biswas, E. Vescovo, A. Rybkin, D. Marchenko and O. Rader, *Phys. Rev. Lett.*, 2008, **101**, 157601.
- 68 C. Gong, G. Lee, B. Shan, E. M. Vogel, R. M. Wallace and K. Cho, *J. Appl. Phys.*, 2010, **108**, 123711.
- 69 L. Köhler and G. Kresse, *Phys. Rev. B*, 2004, **70**, 165405.
- 70 M. Monti, B. Santos, A. Mascaraque, O. Rodríguez De La Fuente, M. A. Niño, T. O. Mentes, A. Locatelli, K. F. McCarty, J. F. Marco and J. De La Figuera, *J. Phys. Chem. C*, 2012, **116**, 11539.
- 71 R. Addou, A. Dahal and M. Batzill, *Nat. Nanotechnol.*, 2013, **8**, 41.
- 72 O. V. Yazev, L. Helm, *Phys. Rev. B*, 2007, **75**, 125408.